THE JOURNAL OF BIOLOGICAL CHEMISTRY VOL. 280, NO. 40, pp. 34080–34087, October 7, 2005

Crystal Structures Representing the Michaelis Complex and the Thiouronium Reaction Intermediate of *Pseudomonas aeruginosa* Arginine Deiminase*

Received for publication, May 18, 2005, and in revised form, July 27, 2005 Published, JBC Papers in Press, August 9, 2005, DOI 10.1074/jbc.M505471200

Andrey Galkin[‡], Xuefeng Lu[§], Debra Dunaway-Mariano[§], and Osnat Herzberg[‡1]

From the [‡]Center for Advanced Research in Biotechnology, University of Maryland Biotechnology Institute, Rockville, Maryland 20850 and the [§]Department of Chemistry, University of New Mexico, Albuquerque, New Mexico 87131

L-Arginine deiminase (ADI) catalyzes the irreversible hydrolysis of L-arginine to citrulline and ammonia. In a previous report of the structure of apoADI from *Pseudomonas aeruginosa*, the four residues that form the catalytic motif were identified as Cys^{406}, His^{278}, Asp^{280}, and Asp^{166}. The function of Cys^{406} in nucleophilic catalysis has been demonstrated by transient kinetic studies. In this study, the structure of the C406A mutant in complex with L-arginine is reported to provide a snapshot of the enzyme·substrate complex. Through the comparison of the structures of apoenzyme and substrate-bound enzyme, a substrate-induced conformational transition, which might play an important role in activity regulation, was discovered. Furthermore, the position of the guanidinium group of the bound substrate relative to the side chains of His^{278}, Asp^{280}, and Asp^{166} indicated that these residues mediate multiple proton transfers. His^{278} and Asp^{280}, which are positioned to activate the water nucleophile in the hydrolysis of the *S*-alkylthiouronium intermediate, were replaced with alanine to stabilize the intermediate for structure determination. The structures determined for the H278A and D280A mutants co-crystallized with L-arginine provide a snapshot of the *S*-alkylthiouronium adduct formed by attack of Cys^{406} on the guanidinium carbon of L-arginine followed by the elimination of ammonia. Asp^{280} and Asp^{166} engage in ionic interactions with the guanidinium group in the C406A ADI·L-arginine structure and might orient the reaction center and participate in proton transfer. Structure determination of D166A revealed the apoD166A ADI. The collection of structures is interpreted in the context of recent biochemical data to propose a model for ADI substrate recognition and catalysis.

L-Arginine is used by a number of pathogenic microorganisms to generate ATP via the arginine dihydrolase pathway (1, 2). Arginine deiminase (ADI[2]; EC 3.5.3.6) (Fig. 1*A*) catalyzes the first step of the pathway, wherein arginine is hydrolyzed to citrulline and ammonia. The gene encoding ADI is absent in humans, whereas the enzyme is essential for the survival of pathogenic protozoa and bacteria. Thus, ADI is an attractive antimicrobial drug target candidate. ADI is also a potential anti-angiogenic agent (3) and an antileukemic and nonleukemic murine tumor agent (4).

We have previously determined the crystal structure of ADI from *Pseudomonas aeruginosa* (PaADI) in its unbound state (5). Despite the lack of significant amino acid sequence homology, the core domain structure is similar to those of other arginine-modifying or substituted arginine-modifying enzymes, N^{ω},N^{ω}-dimethylarginine hydrolase (DDAH) (6), arginine:glycine amidinotransferase (7), arginine:inosamine-phosphate amidinotransferase (8), and human peptidylarginine deiminase (PAD4) (9). Based on the structural similarity and conservation of several key residues in the active site of DDAH and ADI, we proposed a model of arginine binding to ADI in which the guanidinium group is positioned in close proximity to the catalytic Cys^{406} (5). Three other residues are in close proximity to the guanidinium group of the substrate: His^{278}, Asp^{280}, and Asp^{166}. The structural data suggested a nucleophilic attack by the thiol group of Cys^{406} on the guanidinium carbon of the arginine substrate. The role of Cys^{406} in nucleophilic catalysis was supported by demonstrating the formation of a covalent adduct between Cys^{406} and the substrate, using a combination of an intermediate trapping and rapid quench techniques with radiolabeled L-[1-^{14}C]arginine (10). The reactions of either C406A ADI or C406S ADI failed to produce a ^{14}C-labeled intermediate, thereby providing evidence of the essential role of Cys^{406} in nucleophilic catalysis. The structure of the ADI from *Mycoplasma arginii* (McADI) has also been described (11). The enzyme was co-crystallized with arginine, which gave rise to two different complexes, a tetrahedral adduct and a *S*-alkylthiouronium adduct. McADI shares 28% sequence identity with PaADI.

In the present work, we focused on obtaining the structure of the PaADI·L-arginine complex so that we could identify conformational changes that occur upon substrate binding and determine the orientation of substrate binding and catalytic groups in the enzyme·substrate complex. The strategy for structure determination employed the C406A mutant, which we had shown in earlier work to be inactive (10). The C406A-arginine structure guided the design of active site mutants in which substrate activation and/or general acid/base catalysis might be impaired. Specifically the H278A, D166A, and D180A mutants were prepared and subjected to kinetic analysis (the results of which are reported in a separate paper)[3] and to crystallization in the presence of L-arginine followed by x-ray structure determination. The structures reported in this paper, are interpreted in the context of the biochemical data to support a model for PaADI substrate recognition and catalysis.

* Supported by National Institutes of Health Grants P01 GM57890 (to O. H.), R01 AI59733 (to O. H., D. D.-M., and P. S. Mariano), and RO1 GM28688 (to D. D.-M.). The costs of publication of this article were defrayed in part by the payment of page charges. This article must therefore be hereby marked "*advertisement*" in accordance with 18 U.S.C. Section 1734 solely to indicate this fact.

The atomic coordinates and structure factors (codes 2a9g, 2aaf, 2abr, and 2aci) have been deposited in the Protein Data Bank, Research Collaboratory for Structural Bioinformatics, Rutgers University, New Brunswick, NJ (http://www.rcsb.org/).

[1] To whom correspondence should be addressed: Center for Advanced Research in Biotechnology, 9600 Gudelsky Dr., Rockville, MD 20850. Tel.: 240-314-6245; Fax: 240-314-6255; E-mail: osnat@carb.nist.gov.

[2] The abbreviations used are: ADI, arginine deiminase; PaADI, ADI from *Pseudomonas aeruginosa*; McADI, ADI from *Mycoplasma arginii*; Pad4, peptidylarginine deiminase; DDAH, dimethylarginine hydrolase; r.m.s.d., root-mean-square deviation.

[3] X. Lu, L. Li, X. Feng, A. Galkin, O. Herzberg, P. S. Mariano, and D. Dunaway-Mariano, submitted for publication.

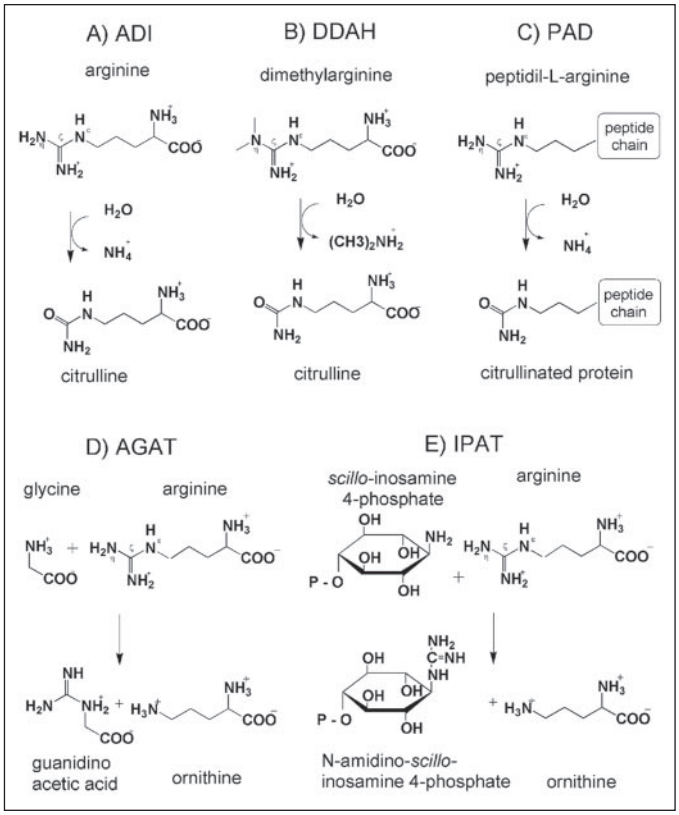

FIGURE 1. **The reactions catalyzed by ADI superfamily members.** *A*, ADI; *B*, DDAH; *C*, PAD; *D*, arginine:glycine amidinotransferase (*AGAT*); *E*, arginine:inosamine-phosphate amidinotransferase (*IPAT*).

MATERIALS AND METHODS

Crystallization and Data Collection—The expression construct pET100/ADIn coding for wild-type untagged protein was used for production of ADI mutants (5). Site-directed mutagenesis was carried out and the recombinant mutant proteins prepared as described elsewhere (10).[3] Crystals of ADI mutants were obtained by the vapor diffusion method in hanging drops at room temperature. Protein solutions containing 20 mM arginine were mixed with an equal volume of mother liquor containing 34–38% 2-methyl-2,4-pentanediol, 6.0–7.0% polyethylene glycol 3350, 0.1 M Tris-HCl (pH 7.6), and 20 mM arginine and equilibrated against the mother liquor reservoir. Crystals appeared within 2–8 weeks and grew to $\sim 0.1 \times 0.1 \times 0.2$ mm^3.

For data collection, the crystals in their solution were flush-cooled in liquid propane cooled in liquid nitrogen. Diffraction data were acquired at 100 K using an RAXIS IV++ image plate detector mounted on a Rigaku rotating anode x-ray generator (Rigaku MSC Inc.). Data processing was carried out using CrystalClear, version 1.3.5 (Rigaku MSC Inc.). The statistics of data collection are provided in TABLE ONE.

Structure Determination and Refinement—The crystal form of the mutant ADIs is different from that of the free ADI. The structures were therefore determined by molecular replacement techniques with the computer program CNS (crystallography NMR software) (13), using the ADI apostructure (Protein Data Bank code 1RXX) as the search model. The difference Fourier maps indicated some alternative tracing. Structure refinement was carried out using the CNS program. The four molecules in the asymmetric unit were refined independently. The resulting models were inspected and modified on a graphics work station using the program O (14). Water molecules were added to the model based on the $F_o - F_c$ difference Fourier electron density map (where F_o and F_c are the observed and calculated structure factors, respectively), using peaks with density $\geq 3\sigma$ as the acceptance criteria. PROCHECK was used for analysis of geometry (15), QUANTA for molecular modeling and structural alignment (Molecular Simulations Inc.), and PYMOL for depiction of the structures (16).

RESULTS AND DISCUSSION

Structure Determinations

The first goal of this work was to obtain a structure of the ADI active site with substrate bound. In a previous study, the C406A mutant, devoid of the active site nucleophile, was shown to be catalytically inert (10). Accordingly, the C406A mutant was co-crystallized with L-arginine at pH 7.6 for x-ray structure determination. The second goal of this work was to probe the role of key catalytic residues (His^{278}, Asp^{280}, and Asp^{166}) and to obtain the structures of ADI at various stages along reaction pathway by co-crystallization of mutants of these residues with L-arginine. The H278A, D280A, and D166A ADI mutants, which catalyze the conversion of L-arginine to citrulline at a negligible rate (10^6–10^7-fold slower than the wild-type enzyme),[3] were co-crystallized with L-arginine at pH 7.6. The x-ray crystal structures obtained are described below.

Overall Structure

Refinement results are summarized in TABLE ONE, and electron density maps in the vicinity of the active side are shown in Fig. 2. All structures of the mutant ADIs contain four protein molecules in the asymmetric unit: A, B, C, and D. The molecules pack into tetramers with approximate 222 symmetry of the noncrystallographic 2-fold symmetry axes. The four ADI structures are as follows.

*The C406A ADI·*L-Arginine Complex—The active site is occupied by an intact L-arginine (Fig. 2*A*). The model includes 1618 amino acid residues and 1064 water molecules. Pairwise superposition of monomers results in a root-mean-square deviation (r.m.s.d.) between the α-carbon positions of 0.4 Å. The five N-terminal residues of each molecule are not visible in the electron density map. In addition, no electron density is associated with the following surface residues: 345–351, and 418 in molecule A; 275–276, 345–348, and 417–418 in molecule B; 273–275, 345–351, and 418 in molecule C; 346–351 and 418 in molecule D. These residues were omitted from the final model.

H278A ADI·S-Alkylthiouronium Intermediate Complex—The model (Fig. 2B) includes 1626 amino acid residues and 802 water molecules. Superposition of monomers yields a r.m.s.d. of α-carbon positions in the range of 0.4 to 0.8 Å. The five N-terminal residues of each molecule are not visible in the electron density map. In addition, no electron density is associated with the following surface residues: 345–351 and 418 in molecule A; 345–348 in molecule B; 345–350 in molecule C; 345–351 in molecule D. These residues were omitted from the final model.

D280A ADI-S-Alkylthiouronium Intermediate—The model (Fig. 2C) contains 1613 amino acid residues. The crystals obtained for this mutant were fragile and very sensitive to manipulations. They diffracted only to resolution of 2.9 Å and had high mosaic spread (2.3°). Therefore no water molecules were added to the model. The monomers exhibit a r.m.s.d. between superposed α-carbon atoms in the range of 0.4 and 0.5 Å. The five N-terminal residues of each molecule are not visible in the electron density map. In addition, no electron density is associated with the following residues: 274–276, 345–351, and 418 in molecule A; 273–274, 345–348, and 418 in molecule B; 6, 274–275, 345–350, and 418 in molecule C; 275–276, 345–351, and 417–418 in molecule D. These residues were omitted from the final model.

TABLE ONE

X-ray data collection and refinement statistics

	C406A	H278A	D280A	D166A
Data collection				
Space group	$P2_12_12_1$	$P2_12_12_1$	$P2_12_12_1$	$P2_12_12_1$
Unit cell dimensions *a, b, c* (Å)	91.1, 120.7, 151.0	90.8, 121.2, 151.3	90.6, 120.6, 147.2	91.2, 123.9, 150.0
Resolution range (Å)	20–2.3	20–2.3	20–2.9	20–2.5
No. observations	369187	271515	106525	272077
No. unique reflections	73975	73866	34967	55706
Completeness (%)[a]	99.4 (96.1)	98.9 (99.9)	96.2 (97.3)	93.8 (92.4)
*R*merge[a,b]	0.097 (0.272)	0.101 (0.300)	0.103 (0.263)	0.097 (0.361)
Refinement statistics				
No. reflections	73861	73809	34924	55661
No. residues	1618	1626	1613	1620
No. water molecules	1064	802	0	300
*R*cryst[c]	0.199	0.200	0.214	0.198
*R*free[d]	0.267	0.264	0.274	0.272
r.m.s.d.				
Bonds (Å)	0.013	0.016	0.024	0.015
Angles (°)	1.9	2.0	2.3	1.9
Average B-factor (Å^2)	37	36	45	41
Ramachandran plot (%)				
Most favored	89.9	89.7	85.2	87.2
Allowed	9.5	9.8	14.2	12.1
Generously allowed	0.6	0.5	0.6	0.7
Disallowed	0.0	0.0		0.0

[a] The values in parentheses are for the highest resolution shell.
[b] *R*merge = $\Sigma_{hkl}[(\Sigma_j|I_j - \langle I\rangle|)/\Sigma_j|I_j|]$, for equivalent reflections.
[c] *R*cryst = $\Sigma_{hkl}||F_o|-|F_c||/\Sigma_{hkl}|F_o|$, where F_o and F_c are the observed and calculated structure factors, respectively.
[d] *R*free is computed for 5% of reflections that were randomly selected and omitted from the refinement.

ApoD166A ADI—The model (Fig. 2D) contains 1620 amino acid residues and 300 water molecules. The monomers exhibit a r.m.s.d. between superposed α-carbon atoms in the range of 0.4 to 0.5 Å. The five N-terminal residues of each molecule are not visible in the electron density map. In addition, electron density is missing for the following residues: 273–275, 345–351, and 418 in molecule A; 345–348 in molecule B; 6, 274–275, 345–350, and 418 in molecule C; 345–351 in molecule D. These residues were omitted from the final model.

Pairwise superposition of the free wild-type ADI and the mutant enzyme·substrate complexes show that the overall fold of the structures remains similar, yet with some local changes that result in r.m.s.d. values between α-carbon atoms that range between 0.6 and 0.8 Å. In particular, four loops associated with the active site undergo conformational transitions not related to crystal packing: loop 1 comprising residues 30–46, loop 2 comprising residues 178–185, loop 3 comprising residues 271–281 (part of this loop is disordered in the apoADI structure), and loop 4 comprising residues 393–404 (Fig. 3*A*). Residues adjacent to the substrate exhibit the most significant shifts. For example, the α-carbon atom of Leu^{41} (loop 1) shifts by 2.7 Å and that of Arg^{185} (loop 2) by 1.8 Å; the α-carbon atom of His^{278} (loop 3) shifts by 0.9 Å and that of Gly^{400} (loop 4) by 4.4 Å. These are localized but mechanistically important conformational transitions that tighten the surrounding of the substrate. Simultaneously, substrate binding is accompanied by displacement of the side chain of Arg^{401} (loop 4) by more than 8 Å to enable access to the active site (Fig. 3*B*). The significance of the Arg^{401} side chain movement is discussed below.

Substrate Binding Site

The difference Fourier electron density maps clearly show bound ligands for three mutant ADIs, C406A, H278A, and D280A, but not for the D166A mutant (Fig. 2). The structure of the H278A ADI complex was refined at higher resolution than that of D280A ADI, and both represent a *S*-alkylthiouronium reaction intermediate in which the guanidinium group of the L-arginine substrate forms an amidino adduct with Cys^{406}. In the following discussion, the more accurate H278A ADI structure is used for illustration.

The ADI active site lies in the center of a barrel formed by a cyclic arrangement of five ββαβ modules (Fig. 3*A*). Residues involved in a hydrogen bonding network with L-arginine are shown in Fig. 4. As discussed previously (5, 11), the ADI active site organization is similar to that of the other enzymes of the superfamily: DDAH, PAD4, arginine:inosamine-phosphate amidinotransferase, and arginine:glycine amidinotransferase. However, the substrate orientation in arginine:glycine amidinotransferase and arginine:inosamine-phosphate amidinotransferase is different compared with that of DDAH (6, 7), PAD4 (9), and ADI. Arginine:glycine amidinotransferase and arginine:inosamine-phosphate amidinotransferase catalyze the amidino group transfer of arginine to a second substrate, producing the amidino derivatives of the substrates and ornithine (Fig. 1). The Cζ–Nε bond of the arginine is cleaved in these reactions. In contrast, DDAH, PAD4, and ADI are hydrolytic enzymes, catalyzing the Cζ–Nη bond cleavage.

In ADI, the L-arginine substrate binds such that the guanidinium group exposes opposite faces to the Cys^{406} and His^{278} side chains (Fig. 4, *A* and *B*). In the H278A and D280A ADI structures, the Cys^{406} sulfur atom is covalently linked to the guanidinium group Cζ atom of the substrate, replacing its NH_2 substituent. In the C406A, H278A, and D280A ADI structures, the guanidinium group of the ligand interacts with the carboxylate groups of Asp^{166} and Asp^{280} (except that one carboxylate group is missing in D280A ADI). The aliphatic portion of the ligand interacts with Phe^{163} (Fig. 2, *A–C*), and the Cα-carboxyl group

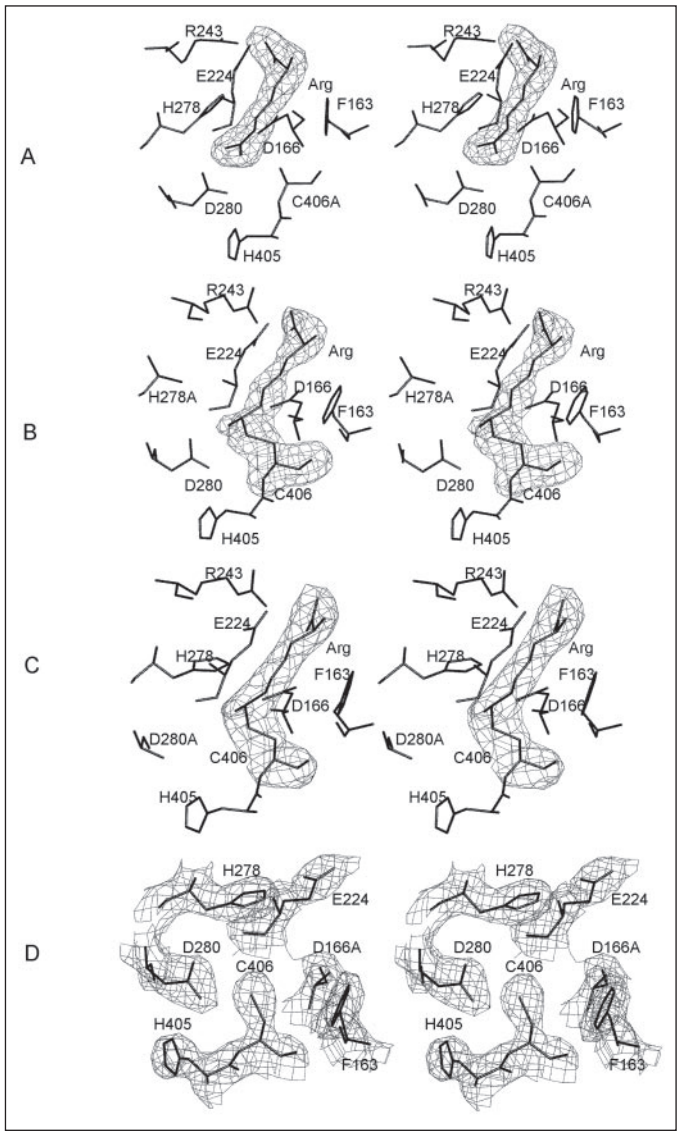

FIGURE 2. **Stereoscopic view of the electron density in the vicinity of the active site.** *A*, C406A ADI mutant; *B*, H278A ADI mutant; *C*, D280A ADI mutant; *D*, D166A ADI mutant. *A–C*, difference electron density maps with the coefficients $F_o - F_c$ were calculated prior to inclusion of the ligand in the model. The maps are countered at the 3σ level. *D*, difference electron density map with the coefficients $2F_o - F_c$ is shown countered at the 1σ level.

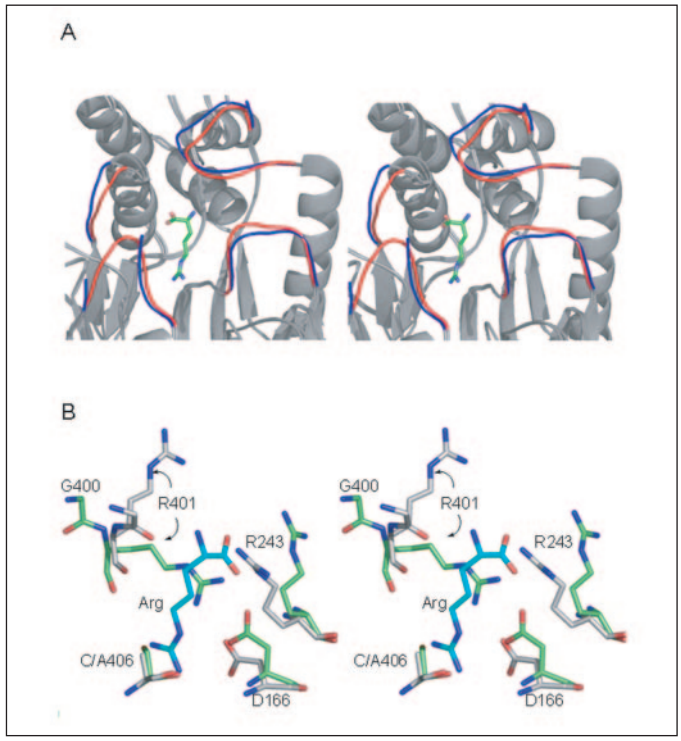

FIGURE 3. **Stereoscopic view of ADI in the unbound and bound states.** *A*, the superposed molecules are colored *gray* where the trace of the polypeptide chain is similar in both structures. For regions exhibiting differences, loops of the apoADI structure are highlighted in *blue*, and loops of the ADI structure complexed with arginine are highlighted in *red*. *B*, close-up view of the conformational transition that active site residues undergo upon substrate binding. The arginine substrate is shown in *cyan*. The carbon atoms of the apostructure are colored *green*. Other atomic colors are as follows: oxygen, *red*; nitrogen, *blue*; carbon, *gray*.

forms ionic interactions with Arg^{185} and Arg^{243} (Fig. 4, *A* and *B*). The Cα-amino group of the ligand is fixed by electrostatic interactions with the main chain oxygen atoms of Leu^{41} and Gly^{400} and with the oxygen atom of the amide group of Asn^{160}. Enzyme activity is exquisitely sensitive to amino acid replacements of the polar substrate binding residues, as demonstrated elsewhere.[3]

Reaction Mechanism and the Role of Mutated Residues

The overall reaction catalyzed by ADI is the hydrolytic substitution of the ηNH_2 group from the guanidinium group Cζ of L-arginine, leading to citrulline and ammonia (Fig. 1). The role of Cys^{406} in nucleophilic catalysis is well supported by experimental data. First, single turnover reactions carried out with PaADI and L-[^{14}C]arginine have demonstrated a kinetically competent covalent enzyme intermediate that forms in the wild-type ADI but not in the C406A or C406S ADI mutants (10). The covalent adduct was presumed to be the Cys^{406}-*S*-alkythiouronium intermediate (Fig. 5, depicted in *complexes III* and *IV*). The x-ray structure of the C406A ADI·L-arginine complex, described in the previous section, shows that the side chain of the Cys^{406} residue would be positioned for addition to the guanidinium group Cζ of the L-arginine ligand in the enzyme·substrate complex.

Second, Arnold and co-workers (11) observed intermediates linked to the active site cysteine of wild-type McADI. One intermediate was the tetrahedral adduct (Fig. 5, *complex V*), and the second was the Cys-*S*-alkythiouronium intermediate (Fig. 5, *complex IV*) attributed to the back reaction that occurs when citrulline accumulates. Third, in a recent study of the reaction of DDAH with the substrate analog *S*-methyl-L-thiocitrulline, the Cys^{249}-*S*-alkythiouronium intermediate was captured at steady state by acid quench and characterized by electrospray ionization mass spectrometry (17).

Fourth, in this study we have determined the structure of the PaADI Cys^{406}-*S*-alkythiouronium intermediate formed by co-crystallization of L-arginine and the H278A or D280A mutant emzymes. Solution studies show that the rate of citrulline formation by these two mutants is extremely slow,[3] which indicates that without the His^{278} or without the Asp^{280} residues, ADI is unable to hydrolyze the Cys^{406}-*S*-alkythiouronium intermediate efficiently. Finally, the demonstrated stability of the *S*-alkythiouronium model in water and in aqueous acid[3] indicates that the covalent adduct observed in the crystal is indeed the thiouronium intermediate and not the Cys^{406}-*S*-alkylthiocabamate adduct formed as a dead-end product by *in situ* hydrolysis of the *S*-alkythiouronium intermediate. It follows that the hydrolysis of the *S*-alkythiouronium intermediate requires activation of the water nucleophile.

The active site is enriched with charged and polar groups, and the ionization states of the key catalytic residues are unknown. In previous work we have shown that the PaADI is optimally active at acidic pH

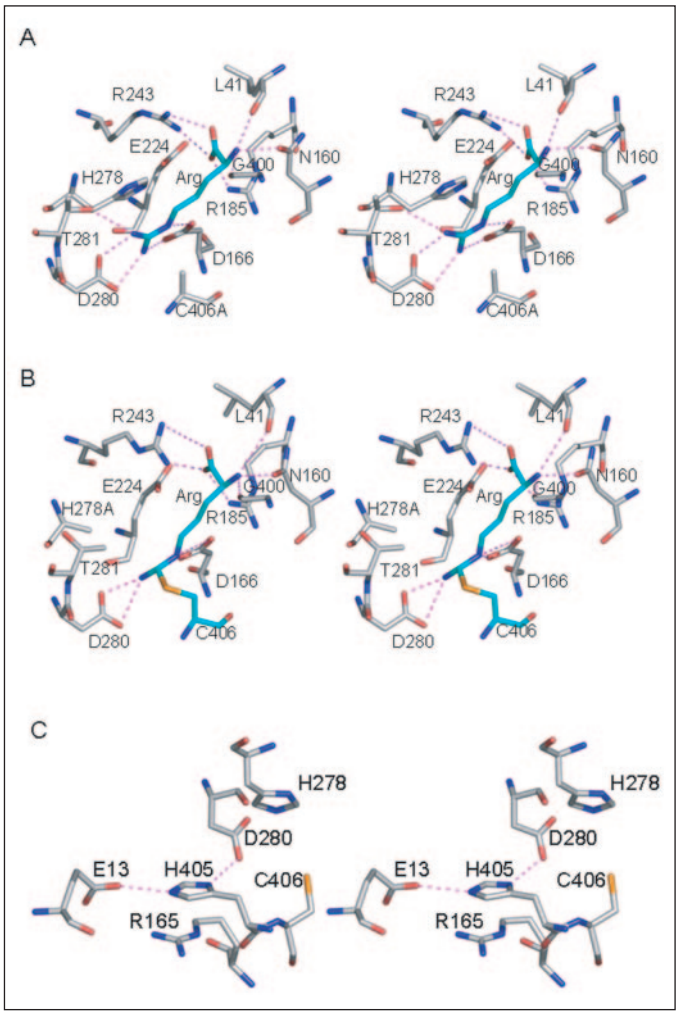

FIGURE 4. **Binding of arginine to ADI mutants and associated interactions.** Atomic colors are as follows: oxygen, *red*; nitrogen, *blue*; carbon, *gray*; sulfur, *yellow*. The carbon atoms of the arginine substrate and the residue representing the thiouronium intermediate are colored *green*. Key interactions are highlighted as *dashed lines*. *A*, stereoscopic representation of C406A ADI·arginine complex. *B*, stereoscopic representation of arginine covalently linked to H278A ADI as *S*-alkythiouronium intermediate. *C*, stereoscopic representation of the charge network extending from Asp^{280} to His^{405}, Glu^{13}, and Arg^{165}.

(below pH 6), and yet *Mycoplasma arthritidis* ADI is known to function at or above pH 7 even though the two enzymes utilize the same constellation of catalytic groups (18). When the L-arginine binds to PaADI, the positively charged guanidinium group is positioned in between His^{278} and Cys^{406} and thereby perturbs the local electrostatic environment of these catalytic groups. The ionization state of His^{278} is further modulated by its electrostatic interaction with Glu^{224}, which we know from kinetic analysis of the E224D and E224A mutants to contribute 3 orders of magnitude to the turnover rate (k_{cat}).[3] Asp^{280} is also involved in an intricate interaction network, which includes the buried residues His^{405}, Arg^{165}, and Glu^{13} (Fig. 4*C*). Of these four residues, Asp^{280} and Glu^{13} are invariant in all known ADIs, and His^{405} is sometimes replaced by an arginine, as in the case of McADI. The precise side chain orientation and the network of interactions indicate that His^{405} shares protons with Asp^{280} and with Glu^{13} and is likely to be protonated. This may explain the low pH optimum of PaADI (5.6) in contrast to the neutral pH optimum of McADI, the enzyme that contains an arginine residue instead of His^{405}. The presence of another invariant residue, Arg^{165}, in which the guanidinium group stacks against the His^{405} imidazolium ring, further complicates the charge distribution (Fig. 4*C*). This is an exquisite arrangement, in which the position of the guanidinium group is supported by the interaction of one ηNH_2 atom with Thr^{408} Oγ, the second ηNH_2 interacting with an internal water molecule bridged to Glu^{13}, and the Nϵ atom interacting with His^{405} backbone carbonyl. A survey of the Protein Data Bank showed that the stacking of His-Arg side chains is the most commonly observed geometry of such pairs (19). We speculate that the stacking of the Arg^{165}-His^{405} pair is mediated by π electrons and dictates the precise positioning of the imidazolium ring of His^{405} between the two acidic groups of Glu^{13} and Asp^{280}, which in turn fixes the orientation of Asp^{280} carboxyl group with respect to the guanidinium group of the substrate.

Based on the new information provided by the structures of the complexes, we have modified slightly the previous reaction mechanism proposed by us (5) and independently by Arnold and colleagues (11). We might assume that the first step is initiated by the Cys^{406} thiolate group mounting a nucleophilic attack on the guanidinium group Cζ atom, leading to the tetrahedral intermediate (Fig. 5, *complex II*). This step is followed by a proton transfer to the ηNH_2 group, cleavage of the Cζ–Nη bond, and the formation of the Cys^{406}-*S*-alkylthiouronium intermediate concomitant with release of NH_3 (Fig. 5, *complex III*). Acid catalysis is required, and the structures of the McADI tetrahedral adduct and of the C406A PaADI·L-arginine complex show that His^{278} is best oriented for this role. The implication is that His^{278} is positively charged. The role of His^{278} in acid catalysis is consistent with, but not dictated by, the reduction in rate of *S*-alkylthiouronium intermediate formation observed with the H278A PaADI.[3]

The roles of Asp^{166} and Asp^{280} appear to be different, although both are required for citrulline formation.[3] The observation that D166A PaADI does not co-crystallize with the L-arginine is consistent with its role in substrate binding, which is evident from the structure of the C406A-PaADI·L-arginine complex. In contrast, D280A PaADI binds L-arginine to produce the *S*-alkylthiouronium intermediate, indicating that its primary role is in enhancement of the nucleophilicity of the Cζ atom and activation of the hydrolytic water molecule, as described below, and not in countering the charge of the L-arginine guanidinium group. The kinetic characterization using [^{14}C]arginine supports the crystallographic results, as it shows no accumulation of [^{14}C]D166A ADI, in contrast to the accumulation of [^{14}C]D280A enzyme.[3]

Next, the departing NH_3 is replaced by a hydrolytic water molecule. In PaADI, His^{278} is positioned to bind and deprotonate the water nucleophile, and the analogous residue in McADI is His^{269}. The *S*-alkylthiouronium intermediate of McADI revealed a water molecule hydrogen bonded to both His^{269} and Asp^{271} (equivalents of His^{278} and Asp^{280} in PaADI), which suggests that both residues are responsible for the activation of the water molecule (11). We do not see such a water molecule in the structures of PaADI *S*-alkylthiouronium intermediate, perhaps because both His^{278} and Asp^{280} are required for anchoring the water molecule and polarizing it for nucleophilic attack. We note that in McADI, this water molecule is also mobile, with substantially higher crystallographic temperature factor (>35 Å^2) than those of the histidine and aspartate residues (10 Å^2 and lower). The water molecule is missing in three of the four molecules of the asymmetric unit in the structure of PaADI C406A·L-arginine complex. Only in one molecule (molecule D in the Protein Data Bank entry), a water molecule is hydrogen-bonded to His^{278}, but not to Asp^{280}, and could potentially move to the appropriate position upon formation of the *S*-alkylthiouronium intermediate. The absence of the hydrolytic water molecule in the structures of the H278A and D280A PaADI *S*-alkylthiouronium intermediates is consistent with abolishing enzyme activity.[3]

The origin of the *S*-alkylthiouronium intermediate seen with the

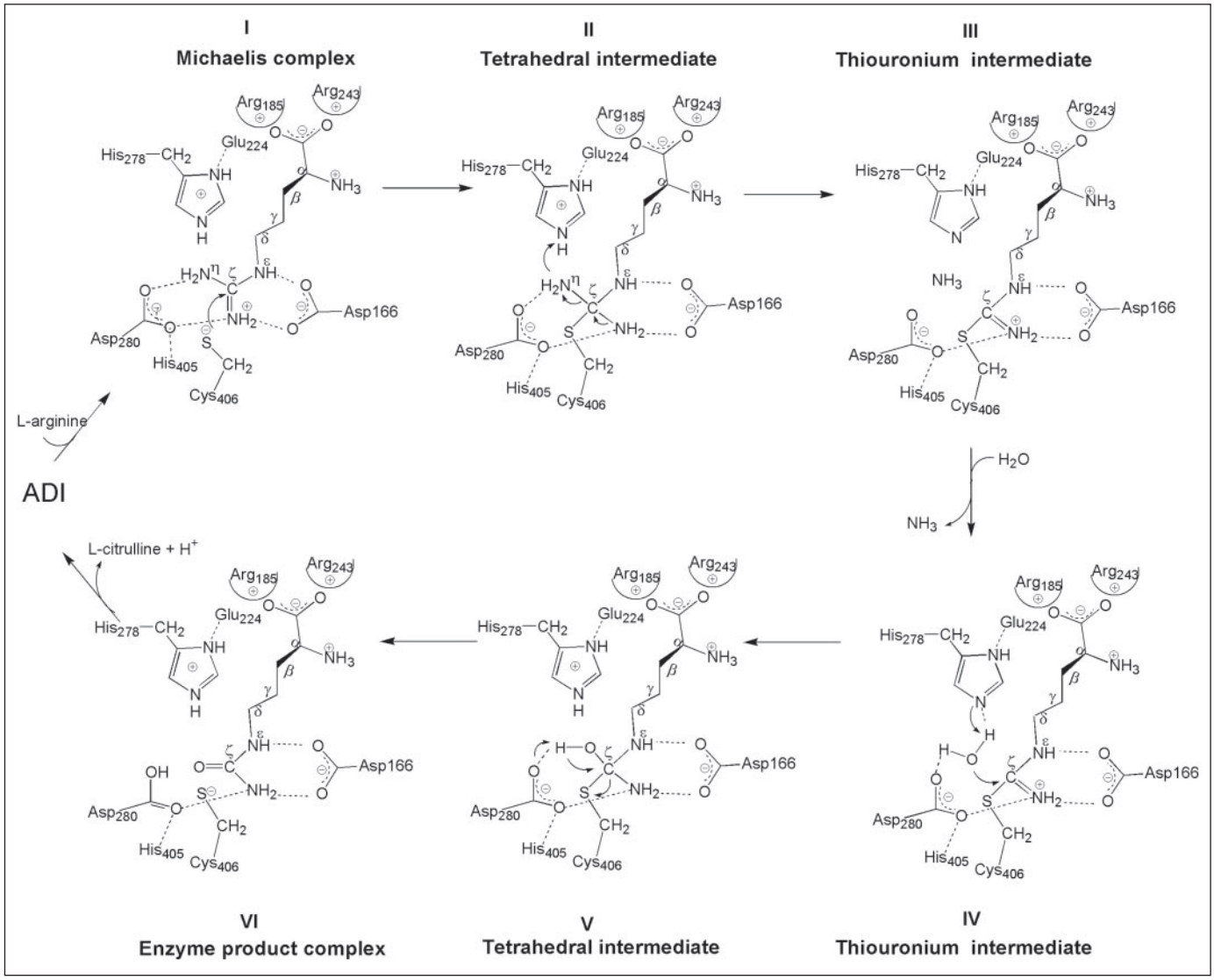

FIGURE 5. **A feasible mechanism of PaADI catalysis of L-arginine hydrolysis to citrulline and ammonia.**

wild-type McADI structure was attributed to the backward reaction once citrulline was formed (11). [^{14}C]Citrulline was used to show that this is not the case with the PaADI mutant complexes as labeled enzyme was not detected.[3] We may conclude, therefore, that the structures of the *S*-alkylthiouronium intermediates of PaADI have arisen from the forward reaction. Because accumulated intermediate was trapped in the crystals of either the His^{278} or Asp^{280} mutant, it appears that elimination of these residues is more detrimental to the second half of the reaction than to the first half. This implies that both residues are crucial for activation of the hydrolytic water molecule.

It is worth noting that although the proposed mechanism uses an ionized catalytic cysteine (Fig. 5), the ionization state of Cys^{406} in the free enzyme remains unknown. If the cysteine is uncharged prior to substrate binding, it would transfer its proton, most likely to solvent, when the guanidinium group of L-arginine approaches. Similarly, the formation of citrulline requires that a proton be removed from the hydroxyl group of the tetrahedral intermediate V (Fig. 5). Either Asp^{280} or Cys^{406} is favorably located for accepting the proton; in Fig. 5 we depict a proton transfer to Asp^{280}. As citrulline diffuses out of the active site, the proton might be released to solvent. If the proton is transferred to Cys^{406}, the thiolate group would be formed upon L-arginine binding.

For the closely related enzyme DDAH, the proposed catalytic mechanism also invoked a nucleophilic attack by a thiolate species and a proton transfer from the imidazolium group (6). The DDAH environment that might facilitate the ionization of the catalytic cysteine differs somewhat from that in ADI, as described below.

Substrate-induced Fit in PaADI Catalysis

The ensemble of structures available for PaADI implies that in *P. aeruginosa*, L-arginine binding is accompanied by an enzyme conformational transition that enables substrate access to the active site. The structure of the apoPaADI shows that in the absence of substrate, the Arg^{401} side chain projects into the active site where it is stabilized through ion pair interaction with the carboxylate group of Asp^{166}. The L-arginine substrate must displace the Arg^{401} side chain to form a productive enzyme·substrate complex. Upon substrate binding the guanidinium group of Arg^{243} shifts by ~5 Å to form an electrostatic interaction with the carboxyl group of the L-arginine substrate (Figs. 3*B* and 4, *A* and *B*), and the Arg^{401} side chain moves to provide a solvent barrier at the active site entrance. It is tempting to speculate that the apparent competition between substrate and the Arg^{401} side chain for the Asp^{166} might serve to reduce the affinity of the PaADI for its substrate without

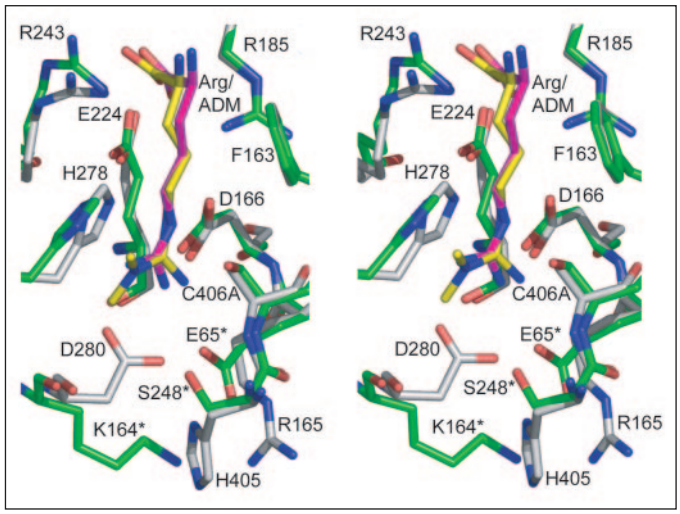

FIGURE 6. **Structural relationship between ADI and DDAH.** Stereoscopic view of superposed active site residues of ADI (*gray*) and DDAH (*cyan*) is shown. Oxygen and nitrogen atoms are colored *red* and *blue*, respectively. The C249S mutant DDAH in complex with N^{ω},N^{ω}-dimethylarginine (*ADM*) and the C406A mutant of ADI in complex with L-arginine (*Arg*) were used. Carbon atoms of Arg are colored *magenta*, and carbon atoms of ADM are colored *yellow*. Only ADI residues are labeled, with the exception of three DDAH residues that differ from their ADI counterparts, which are labeled with an *asterisk*.

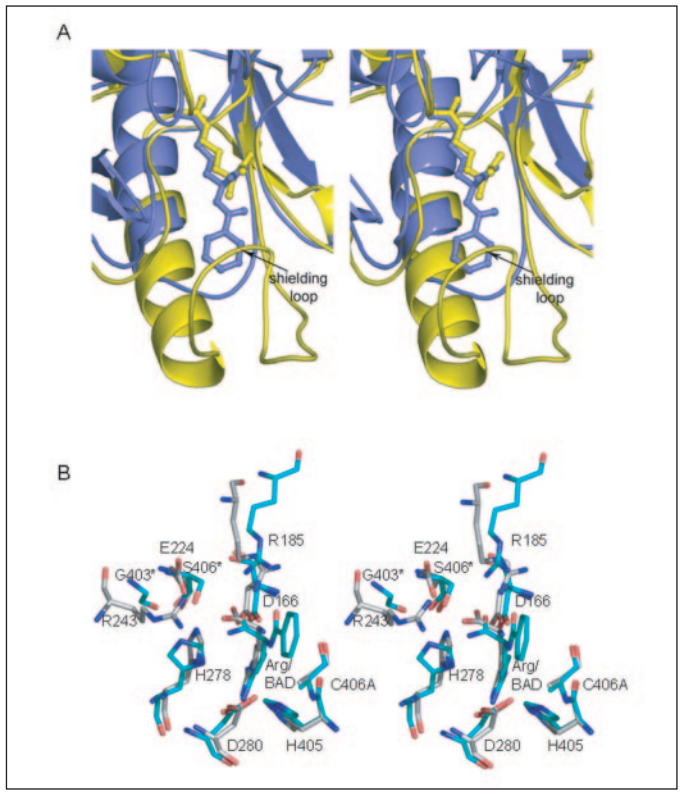

FIGURE 7. **Structural relationship between ADI and PAD4.** The C645A PAD4 in complex with benzoyl-L-arginine amide (*BAD*) and the C406A ADI in complex with arginine were used. *A*, stereoscopic view of superposed active site residues of ADI (*yellow*) and PAD4 (*blue*). *B*, close-up view of the superposed active site residues of ADI (*gray*) and PAD4 (*cyan*). ADI residues are labeled, except that two PAD4 residues that differ from their ADI counterpart are labeled with an *asterisk*.

reducing the ability of the enzyme to orient and activate the substrate once it is bound. Whereas the K_m of the PaADI is 140 μM, the K_m of the *Mycoplasma* ADI (which contains a methionine, not arginine, at the same position) is 4 μM. The PaADI is therefore less likely to drain the cellular reserve of L-arginine for energy production when L-arginine levels are especially low.

Origin of Substrate Specificity

ADI (5, 11), DDAH (6), PAD4 (9), arginine:inosamine-phosphate amidinotransferase (8), and arginine:glycine amidinotransferase (7) are members of a superfamily that carry out related chemical reactions (Fig. 1) and share overall fold and active site architecture. The amidinotransferases, arginine:inosamine-phosphate amidinotransferase and arginine:glycine amidinotransferase, break a different bond than do the hydrolases, ADI, DDAH, and PAD4 (Cϵ–Nη *versus* Cζ–Nη, respectively). As noted previously (11), the target scissile bond of the substrate is placed in the same orientation with respect to the cysteine and the histidine catalytic residues; therefore, substrates bind to the transferases in a different orientation than they bind to the hydrolases. Because of the closer similarity of the hydrolases, ADI is compared here with the structures of the C249S mutant DDAH in complex with N^{ω},N^{ω}-dimethylarginine (6) and the C645A mutant PAD4 in complex with benzoyl-L-arginine amide (9).

The structural basis of substrate specificity of the two *P. aeruginosa* enzymes, ADI and DDAH, is of particular interest. Their substrates are quite similar (Fig. 1), yet the enzymes discriminate between them. Moreover, in contrast to ADI, DDAH is also present in humans, where it is involved in modulation of nitric oxide generation (20). Given the close relationship between the two enzymes, it is important that ADI inhibitors that are developed as potential antimicrobial therapeutics do not interfere with DDAH activity.

The superposition of 10 active site residues of ADI and DDAH and the respective bound substrates (Fig. 6) shows that seven of the 10 residues are conserved and overlap closely. The remaining three residues are not conserved and might potentially be responsible for discrimination between methylated and nonmethylated arginine. Asp^{280}, His^{405}, and Arg^{165} in ADI are replaced by Lys^{164}, Ser^{248}, and Glu^{65} in DDAH, respectively (Fig. 6). The superposition shows that if an aspartic acid was positioned at residue 164 of DDAH, as seen in ADI (Asp^{280}), the carboxyl group would hinder binding of N^{ω},N^{ω}-dimethylarginine to DDAH. Instead, the side chain of Lys^{164} in DDAH is oriented away from the N^{ω},N^{ω}-dimethylarginine, forming electrostatic interaction with the carboxyl group of Glu^{65}, the spatial equivalent of Arg^{165} in ADI. To avoid a clash with Lys^{164} of DDAH, a serine residue, Ser^{248}, replaces His^{405} of ADI. This arrangement creates space to accommodate the two methyl groups of N^{ω},N^{ω}-dimethylarginine, and the aliphatic part of the side chain of Lys^{164} contributes to the hydrophobic environment surrounding the methylated guanidinium group of N^{ω},N^{ω}-dimethylarginine.

Comparison of the ADI and DDAH active site environments indicates that an alternative arrangement of functional groups in DDAH might serve to stabilize a thiolate form of the Cys nucleophile. The carboxylate group of Glu^{65} in DDAH is positioned similar to Asp^{280} in ADI. DDAH Glu^{65} interacts both with the amino group of Lys^{164} (Fig. 6) and the guanidinium group of Arg^{253}, which in turn interacts with Ser^{251} (not shown). Unlike ADI Asp^{280}, Glu^{65} interacts only with the nonmethylated Nη of the substrate and is not in position to participate in the activation of the hydrolytic water molecule.

PAD4, a human protein-arginine deiminase, catalyzes the conversion of protein arginine residues to citrulline (Fig. 1). This posttranslational modification process of target proteins plays a crucial regulatory role in cell development and differentiation (9). Here again, antimicrobial drug development that targets ADI must avoid unwanted targeting of PAD4.

Although PAD4 and ADI share the same overall fold and very similar active sites, PAD4 does not convert free arginine to citrulline, and ADI

does not act on protein-arginine residues. The superposition of ADI and PAD4 (Fig. 7) shows that the ADI active site is shielded from the solvent by a long loop (residues 25–48 in PaADI) and the following two turns of α-helix I (residues 49–56). In the absence of these structural elements, the active site of PAD4 is open and accessible to macromolecules. The superposition of the substrates and eight active site residues shows that six residues are conserved (Fig. 7*B*). The remaining two residues, Glu^{224} and Arg^{243} in ADI, are substituted by smaller residues in PAD4, Ser^{406} and Gly^{403}. In ADI, the positively charged guanidinium group of Arg^{243} interacts with the carboxylate group of the free arginine substrate. The discrimination between substrates in this case arises because there is no need for such an interaction when the arginine is incorporated into a polypeptide chain.

Finally, PAD4 differs from other superfamily members in that its catalytic histidine residue, His^{471}, does not interact with a carboxylate group (Glu^{224} in ADI). Instead, the Nδ atom of the imidazole ring is hydrogen-bonded to Ser^{406} Oγ and to the main chain carbonyl of Gly^{403}. Information about the identity of the proteins that can be modified by PAD4 is only beginning to emerge (12), and the true physiological substrates are still unknown. It is tempting to speculate that the PAD4 loop containing residues 403–406 undergoes a conformational transition that enables a carboxylate group on a protein substrate to interact with His^{471} and stabilize the imidazolium ion. This could control which arginine residue in which protein is converted into citrulline under physiological conditions.

Acknowledgments—We thank John Moult for useful discussions. We also thank the Keck Foundation for providing generous support for the purchase of x-ray equipment at the Center for Advanced Research in Biotechnology.

REFERENCES

1. Zuniga, M., Perez, G., and Gonzalez-Candelas, F. (2002) *Mol. Phylogenet. Evol.* **25,** 429–444
2. Knodler, L. A., Sekyere, E. O., Stewart, T. S., Schofield, P. J., and Edwards, M. R. (1998) *J. Biol. Chem.* **273,** 4470–4477
3. Beloussow, K., Wang, L., Wu, J., Ann, D., and Shen, W. C. (2002) *Cancer Lett.* **183,** 155–162
4. Wheatley, D. N., and Campbell, E. (2002) *Pathol. Oncol. Res.* **8,** 18–25
5. Galkin, A., Kulakova, L., Sarikaya, E., Lim, K., Howard, A., and Herzberg, O. (2004) *J. Biol. Chem.* **279,** 14001–14008
6. Murray-Rust, J., Leiper, J., McAlister, M., Phelan, J., Tilley, S., Santa Maria, J., Vallance, P., and McDonald, N. (2001) *Nat. Struct. Biol.* **8,** 679–683
7. Humm, A., Fritsche, E., Steinbacher, S., and Huber, R. (1997) *EMBO J.* **16,** 3373–3385
8. Fritsche, E., Bergner, A., Humm, A., Piepersberg, W., and Huber, R. (1998) *Biochemistry* **37,** 17664–17672
9. Arita, K., Hashimoto, H., Shimizu, T., Nakashima, K., Yamada, M., and Sato, M. (2004) *Nat. Struct. Mol. Biol.* **11,** 777–783
10. Lu, X., Galkin, A., Herzberg, O., and Dunaway-Mariano, D. (2004) *J. Am. Chem. Soc.* **126,** 5374–5375
11. Das, K., Butler, G. H., Kwiatkowski, V., Clark, A. D., Jr., Yadav, P., and Arnold, E. (2004) *Structure* (*Lond.*) **12,** 657–667
12. Nakayama-Hamada, M., Suzuki, A., Kubota, K., Takazawa, T., Ohsaka, M., Kawaida, R., Ono, M., Kasuya, A., Furukawa, H., Yamada, R., and Yamamoto, K. (2005) *Biochem. Biophys. Res. Commun.* **327,** 192–220
13. Brunger, A. T., Adams, P. D., Clore, G. M., DeLano, W. L., Gros, P., Grosse-Kunstleve, R. W., Jiang, J. S., Kuszewski, J., Nilges, M., Pannu, N. S., Read, R. J., Rice, L. M., Simonson, T., and Warren, G. L. (1998) *Acta Crystallogr. Sect. D Biol. Crystallogr.* **54,** 905–921
14. Kleywegt, G. J., and Jones, T. A. (1999) *Acta Crystallogr. Sect. D Biol. Crystallogr.* **55,** 941–944
15. Laskowski, R. A., and MacArthur, M. W. (1993) *J. Appl. Crystallogr.* **26,** 283–291
16. DeLano, W. L. (2002) *The PyMOL User's Manual*, DeLano Scientific, San Carlos, CA
17. Stone, E. M., Person, M. D., Costello, N. J., and Fast, W. (2005) *Biochemistry* **44,** 7069–7078
18. Weickmann, J. L., and Fahrney, D. E. (1977) *J. Biol. Chem.* **252,** 2615–2620
19. Bhattacharyya, R., Saha, R. P., Samanta, U., and Chakrabarti, P. (2003) *J. Proteome Res.* **2,** 255–263
20. Leiper, J. M., Santa Maria, J., Chubb, A., MacAllister, R. J., Charles, I. G., Whitley, G. S., and Vallance, P. (1999) *Biochem. J.* **343,** 209–214